Sphingobacterium sp T2 manganese superoxide dismutase catalyzes the oxidative demethylation of polymeric lignin via generation of hydroxyl radical

Goran M. M. Rashid, Xiaoyang Zhang, Rachael C. Wilkinson, Vilmos Fülöp, Betty Cottyn Boitte, Stéphanie Baumberger, Timothy Bugg

ACS chemical biology

Articles

Cite This: ACS Chem. Biol. 2018, 13, 2920−2929

pubs.acs.org/acschemicalbiology

Sphingobacterium sp. T2 Manganese Superoxide Dismutase Catalyzes the Oxidative Demethylation of Polymeric Lignin *via* Generation of Hydroxyl Radical

Goran M. M. Rashid,[†,⊥] Xiaoyang Zhang,[†,⊥] Rachael C. Wilkinson,[‡] Vilmos Fülöp,[‡] Betty Cottyn,[§] Stéphanie Baumberger,[§] and Timothy D. H. Bugg*[,†]

[†]Department of Chemistry and [‡]School of Life Sciences, University of Warwick, Coventry CV4 7AL, United Kingdom

[§]Institut Jean-Pierre Bourgin, INRA, AgroParisTech, CNRS, Université Paris-Saclay, 78000 Versailles, France

Supporting Information

ABSTRACT: *Sphingobacterium* sp. T2 contains two extracellular manganese superoxide dismutase enzymes which exhibit unprecedented activity for lignin oxidation but *via* an unknown mechanism. Enzymatic treatment of lignin model compounds gave products whose structures were indicative of aryl−Cα oxidative cleavage and demethylation, as well as alkene dihydroxylation and alcohol oxidation. ^{18}O labeling studies on the SpMnSOD-catalyzed oxidation of lignin model compound guiaiacylglycerol-β-guaiacyl ether indicated that the an oxygen atom inserted by the enzyme is derived from superoxide or peroxide. Analysis of an alkali lignin treated by SpMnSOD1 by quantitative ^{31}P NMR spectroscopy demonstrated 20−40% increases in phenolic and aliphatic OH content, consistent with lignin demethylation and some internal oxidative cleavage reactions. Assay for hydroxyl radical generation using a fluorometric hydroxyphenylfluorescein assay revealed the release of 4.1 molar equivalents of hydroxyl radical by SpMnSOD1. Four amino acid replacements in SpMnSOD1 were investigated, and A31H or Y27H site-directed mutant enzymes were found to show no lignin demethylation activity according to ^{31}P NMR analysis. Structure determination of the A31H and Y27H mutant enzymes reveals the repositioning of an N-terminal protein loop, leading to widening of a solvent channel at the dimer interface, which would provide increased solvent access to the Mn center for hydroxyl radical generation.

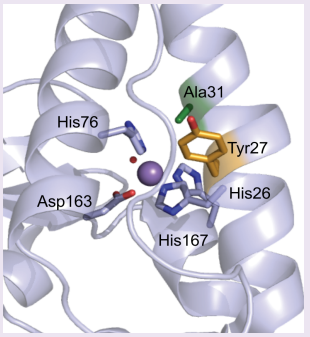

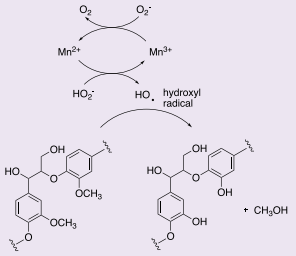

The aromatic heteropolymer lignin is a major constituent (15−25%) of plant cell wall lignocellulose and represents a possible raw material for generation of renewable aromatic chemicals by depolymerization. Although a number of chemical depolymerization methods have been proposed,[1] few biochemical methods are available for lignin depolymerization. Extracellular lignin peroxidase and manganese peroxidase enzymes and multicopper-dependent laccase enzymes from white-rot basiodiomycete fungi are known to oxidize lignin and lignin model compounds,[2] but more recently, bacterial enzymes for lignin degradation have emerged.[3] Bacterial Dyp-type peroxidase enzymes have been identified in *Rhodococcus jostii* RHA1,[4] *Amycolatopsis* sp. 75iv2,[5] and *Pseudomonas fluorescens* Pf-5[6] that can oxidize polymeric lignin, and multicopper oxidases with activity for lignin oxidation have been reported from *Streptomyces coelicolor*[7] and *Ochrobactrum* sp.[8]

Rashid *et al.* have previously identified two extracellular manganese superoxide dismutase enzymes from lignin-degrading bacterium *Sphingobacterium* sp. T2[9] which show activity for oxidation of organosolv and Kraft lignin and lignin model compounds.[10] A number of aromatic products were identified, arising from Cα−Cβ and aryl−Cα oxidative bond cleavage, and a mechanism was proposed involving generation of hydroxyl radical *via* one-electron reduction of hydrogen peroxide.[10] The conventional catalytic mechanism for manganese superoxide dismutase involves reduction of 1 equiv of superoxide to peroxide by Mn(II) and oxidation of a second equivalent of superoxide to dioxygen by Mn(III).[11,12] *Escherichia coli* manganese superoxide dismutase is known not to further reduce peroxide to hydroxyl radical, although the copper/zinc superoxide dismutase can form hydroxyl radical.[13] Nevertheless, precedent for the attack of hydroxyl radical upon lignin can be found in brown-rot fungi, which use Fenton chemistry to produce hydroxyl radical.[14,15] The crystal structure of SpMnSOD1 was determined, but the active site of this enzyme was essentially superimposable upon that of *E. coli* MnSOD, which does not oxidize lignin.[10]

In this paper, we report a more detailed study of the mechanism of oxidation of polymeric lignin and lignin model

Received: June 15, 2018
Accepted: September 24, 2018
Published: September 24, 2018

DOI: 10.1021/acschembio.8b00557
ACS Chem. Biol. 2018, 13, 2920−2929

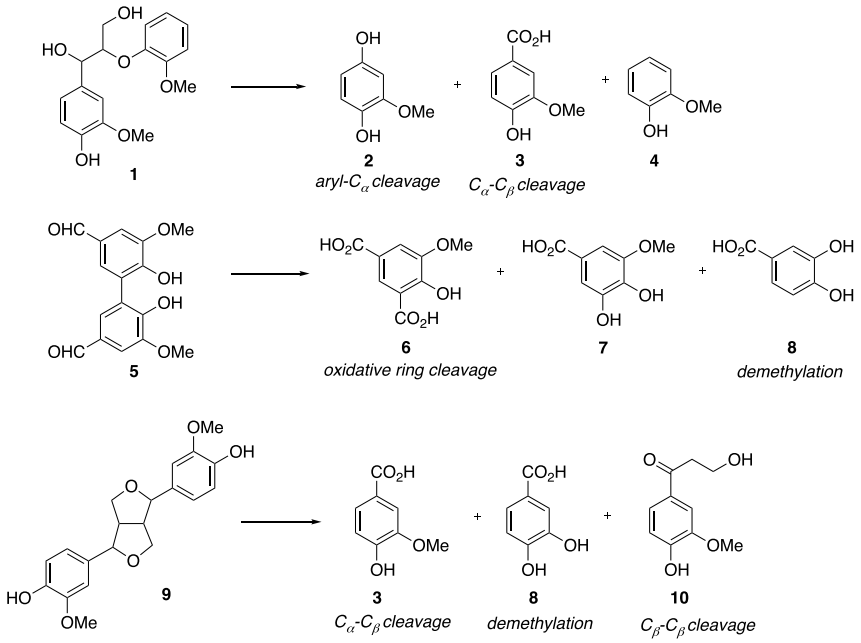

Figure 1. Transformation of dimeric lignin model compounds by SpMnSOD1. GC-MS and LC-MS data for the products identified are shown in Supporting Information (Figures S1−S7).

compounds and the identification of specific amino acid replacements in SpMnSOD1 that are required for the unusual reactivity of this enzyme.

RESULTS

Transformation of Lignin Model Compounds. Recombinant SpMnSOD1 was incubated with several dimeric and monomeric lignin model compounds in the presence of potassium superoxide in DMSO. As reported previously,[10] transformation of *β*-aryl ether lignin dimer **1** by SpMnSOD1 was found to generate methoxyhydroquinone (**2**, GC-MS retention time 19.3 min) *via* oxidative aryl−C*α* bond cleavage, vanillic acid (**3**, GC-MS retention time 22.7 min) *via* oxidative C*α*−C*β* bond cleavage, and guaiacol (**4**, GC-MS retention time 13.8 min), as shown in Figure 1. Transformation of the biphenyl model compound bivanillin (**5**) by SpMnSOD1 was found to generate 5-carboxyvanillic acid (**6**, GC-MS retention time 27.4 min) *via* oxidative ring cleavage, 5-hydroxyvanillic acid (**7**, GC-MS retention time 27.3 min), and protocatechuic acid (**8**, GC-MS retention time 15.8 min). Transformation of *β*−*β* lignin dimer pinoresinol (**9**) by SpMnSOD1 was found to generate vanillic acid (**3**, GC-MS retention time 22.7 min) *via* oxidative C*α*−C*β* cleavage, protocatechuic acid (**8**, GC-MS retention time 15.8 min), and 2-hydroxyethylguaiacylketone (**10**, GC-MS retention time 35.8 min).

Because protocatechuic acid (**8**) was detected in two of the above transformations, its possible formation from demethylation of vanillic acid was studied *via* transformation of vanillic acid (**3**) by SpMnSOD1. Protocatechuic acid was detected, consistent with demethylation activity. 5-Hydroxyvanillic acid (**7**) was also detected, indicative of phenolic hydroxylation, and guaiacol (**4**) formed by decarboxylation (see Figure 2). 3,4-Dimethoxybenzyl alcohol (**11**) was also incubated with SpMnSOD1, generating the corresponding aldehyde (**12**) and acid (**13**) products *via* side chain oxidation and methoxyquinone (**14**).

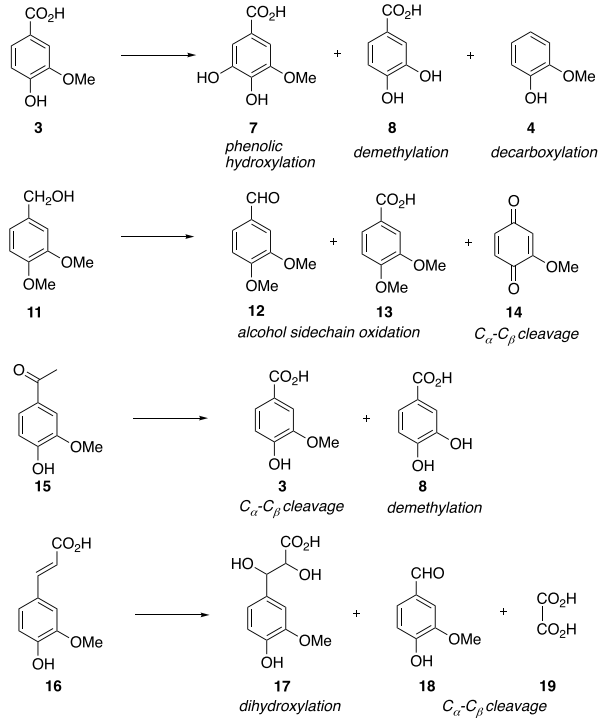

Figure 2. Transformation of monomerc aromatic substrates by SpMnSOD1. GC-MS and LC-MS data for the products identified are shown in Supporting Information (Figures S8−S19).

In order to probe the mechanism of oxidation of pinoresinol (**9**), monocyclic ketone acetovanillone (**15**) was also incubated with SpMnSOD1, generating vanillic acid (**3**), indicating that SpMnSOD1 can catalyze C*α*−C*β* oxidative cleavage of an unactivated C−C bond. Protocatechuic acid (**8**) was also detected, consistent with demethylation of vanillic acid.

Finally, ferulic acid (**16**) was also incubated with SpMnSOD1. A new peak at retention time 29.7 min was

DOI: 10.1021/acschembio.8b00557
ACS Chem. Biol. 2018, 13, 2920−2929

observed, with m/z 229, consistent with the formation of 2,3-dihydroxyphenylpropanoic acid (**17**) *via* dihydroxylation of the alkene functional group of ferulic acid. Vanillin (**18**) and oxalic acid (**19**) were also detected, whose formation could be rationalized *via* oxidative C−C cleavage of acid **17**.

In the case of β-aryl ether **1**, the reaction mechanism was probed further *via* ^{18}O labeling. As SpMnSOD1 is also active using hydrogen peroxide as a substrate, ^{18}O-labeled hydrogen peroxide was generated *in situ* by reaction of $^{18}O_2$ with glucose oxidase and 1 mM glucose. Transformation of lignin model compound **1** by SpMnSOD1 under an atmosphere of $^{18}O_2$ in the presence of glucose oxidase and glucose was found to generate ^{18}O-labeled methoxyhydroquinone **2** (retention time 19.2 min, M^+ 284.6 (disilylated)), with 40.3% ^{18}O incorporation, and ^{18}O-labeled vanillic acid **3** (retention time 22.7 min, M^+ 312.6 (disilylated)), with 39.3% ^{18}O incorporation, consistent with the incorporation of one atom of ^{18}O from hydrogen peroxide into **2** and **3**. The GC-MS spectra for ^{18}O-labeled and unlabeled products are shown in Supporting Information Figure S2.

Evidence for Release of Hydroxyl Radical during SpMnSOD1 Catalysis. Based on the chemical structures of low molecular weight products formed from breakdown of polymeric lignin by SpMnSOD1, Rashid *et al.* previously hypothesized that the lignin oxidation activity of SpMnSOD1 could be caused by the over-reduction of hydrogen peroxide by Mn(II) to hydroxyl radical,[10] a very powerful oxidant that is generated in brown-rot fungi *via* Fenton chemistry in order to attack lignin.[14,15] In order to seek further evidence for hydroxyl radical release, hydroxyphenylfluorescein (HPF) was used as a fluorescence-based assay for hydroxyl radical.[16] Treatment of β-aryl ether model compound with SpMnSOD1 and hydrogen peroxide gave rise to increased fluorescence, compared to that with controls lacking either enzyme or hydrogen peroxide, as shown in Figure 3. Fluorescence signal was dependent upon

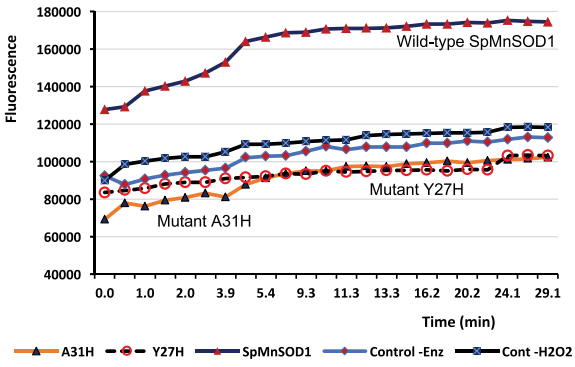

Figure 3. Hydroxyphenylfluorescein assay for hydroxyl radical detection, carried out as described in Experimental Section, using purified SpMnSOD1 or mutant A31H or Y27H enzyme (100 μg) and β-aryl ether lignin model compound (100 μM) and 4 mM hydrogen peroxide in 50 mM phosphate buffer pH 8.0. Control assays contained either no enzyme or no hydrogen peroxide.

protein concentration and hydrogen peroxide concentration (see Supporting Information Figure S20) but was nonlinear versus time, with maximum fluorescence being formed in most assays after 1−2 min. Addition of 5 mM sodium thiosulfate, a quencher for hydroxyl radical,[17] to the assay caused a decrease in observed rate (see Supporting Information Figure S21), and the production of protocatechuic acid from vanillic acid by SpMnSOD1 was inhibited by 70% by addition of 5 mM sodium thiosulfate and inhibited completely by addition of 3 μM hydroxyphenylfluorescein. Calibration of the fluorescence change was carried out using the Fenton reaction using variable concentrations of iron(II) ammonium sulfate with hydrogen peroxide (see Supporting Information Figure S20C),[18] indicating a release of 47 μM hydroxyl radical by 11.4 μM SpMnSOD1, a stoichiometry of 4.1 mol hydroxyl radical per mole of enzyme.

Reaction Co-product and Stoichiometry. The co-product of the enzyme-catalyzed reaction was also investigated. Although demethylase enzymes usually generate formaldehyde *via* oxidation of the methyl group C−H bond, hydroxyl radical has been shown to react with methoxy-substituted aromatic compounds *via* an reaction, with loss of methanol *via* C−O bond cleavage.[19] Attempts to detect formaldehyde using the colorimetric assay of Li *et al.*[20] gave no observed signal from 1,4-dimethoxybenzene and only 2−3 μM formaldehyde from 1 mM vanillic acid (see Supporting Information Figure S22). In contrast, 107 μM methanol was detected *via* oxidation of the methanol produced to formaldehyde, using *Pichia pastoris* alcohol oxidase,[21] followed by acetoacetanilide assay (Supporting Information Figure S22).

Reaction of 1 mM vanillic acid and 4 mM hydrogen peroxide with 11 μM SpMnSOD1 was analyzed. Estimation of hydrogen peroxide concentration using a coupled assay with *P. fluorescens* peroxidase Dyp1B[6] and 2,4-dichlorophenol revealed that 2 mM hydrogen peroxide was consumed, hence after dismutation, 1 mM hydroxyl radical could be formed. HPLC analysis revealed that 110 μM vanillic acid was consumed in the reaction, and that 28 μM protocatechuic acid was formed as the major product, with several minor products formed, including 2-methoxyhydroquinone, guaiacol, and catechol. Hence, we estimate that, of the hydroxyl radical generated by the enzyme, approximately 90% decomposes and 10% reacts with the vanillic acid substrate to form close to 1 equiv of methanol and a range of products, of which protocatechuic acid formed by demethylation is the major product.

Transformation of Polymeric Lignin by SpMnSOD1. Samples of wheat straw organosolv lignin were treated with SpMnSOD1 in the presence of either KO_2/DMSO or H_2O_2 in aqueous buffer, either of which led to the visible solubilization of the lignin samples over 1−4 h (see Supporting Information Figure S23), and samples were analyzed by gel permeation chromatography. Surprisingly, no significant change in apparent M_w was measured (see Table 1): in both cases, the observed M_w had changed by <1% of the value in the absence of oxidant after 1−4 h. Therefore, although some monomeric products are formed,[10] the increased solubility of the lignin polymer could not be explained by a decrease in molar mass of the polymer. Therefore, a more detailed structural inves-

Table 1. Molecular Weight (M_w, g mol^{-1}) Measurement by Gel Permeation Chromatography of Wheat Straw Organosolv Lignin Samples Treated by SpMnSOD1

	KO_2/DMSO	H_2O_2
lignin + buffer	4870	5120
lignin + enzyme + buffer	4970	5060
+oxidant, 1 h	4910	5070
+oxidant, 4 h	4990	5090

DOI: 10.1021/acschembio.8b00557
ACS Chem. Biol. 2018, 13, 2920−2929

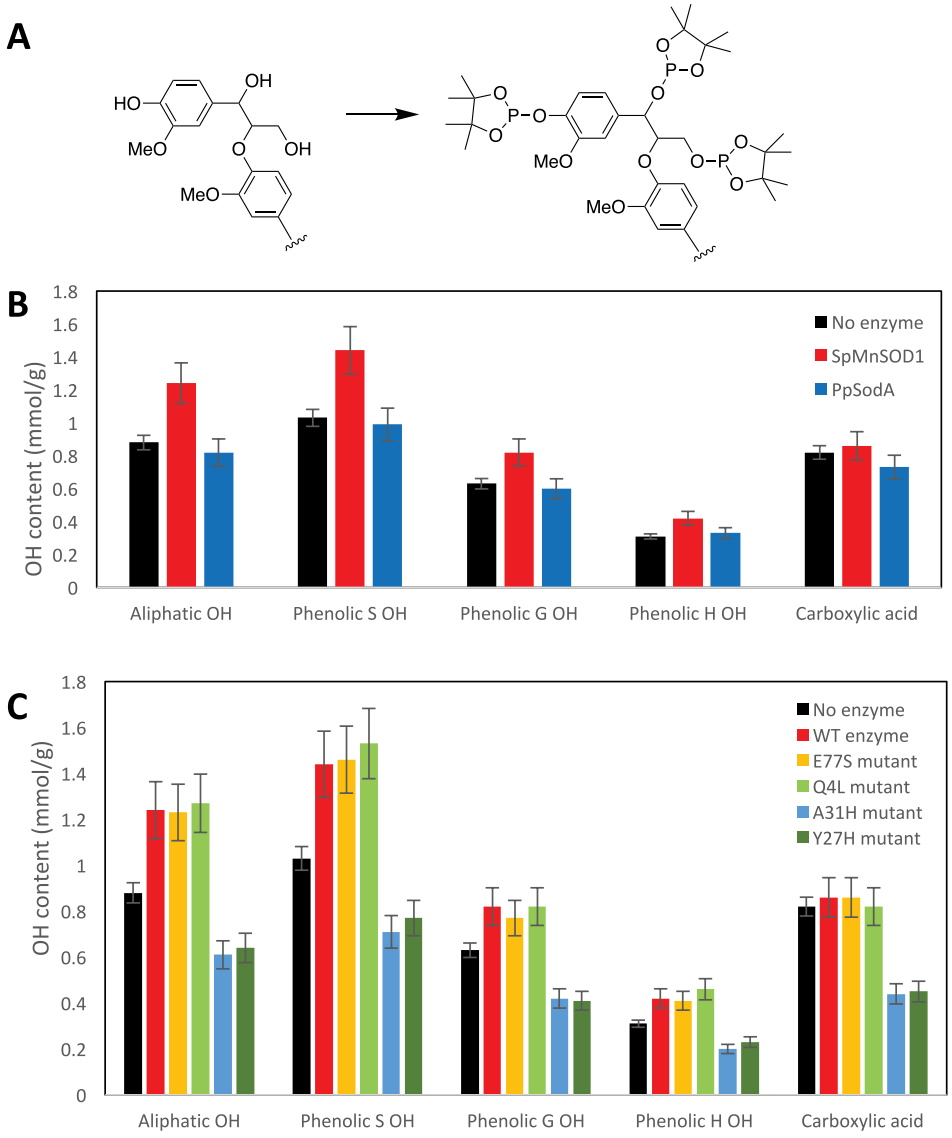

Figure 4. Changes in lignin OH content after treatment by SpMnSOD1. (A) Schematic illustration of phosphitylation method for determination of OH content by ^{31}P NMR spectroscopy. (B) OH content of Protobind alkali lignin before and after treatment by SpMnSOD1 and *P. putida* SodA. (C) OH content of Protobind alkali lignin before and after treatment with wild-type and site-directed mutant SpMnSOD1 enzymes.

Table 2. Partial Amino Acid Sequence Alignment, Showing Amino Acid Replacements in SpMnSOD1 and SpMnSOD2 (Green) Situated Close to Mn Ligands His-26, His-76 (Yellow), and Active Site Residues His-30, Tyr-34, and Asn-75 (Cyan)

	4	26	76
SpMnSOD1	QFKQTPLPYAYDALEGAIDAKTMEIHYSKHAAGYTANLNKAI		GHYNHELFWSILTP
SpMnSOD2	----------MEIHHDRHHQAYVDNLNKAI		GHYNHKLFWSILSP
SODM_THET8	PFKLPDLGYPYEALEPHIDAKTMEIHHQKHHGAYVTNLNAAL		GHLNHSLFWRLLTP
SODM_STRPY	AIILPELPYAYDALEPQFDAETMTLHHDKHHATYVANTDAAL		GHLNHALFWELLSP
SODM_ECOLI	SYTLPSLPYAYDALEPHFDKQTMEIHHTKHHQTYVNNANAAL		GHANHSLFWKGLKK
H6MT45_GORPV	EYTLPDLPYDYAALEPHISGRIMELHHDKHHATYVKGANDTL		GHTNHSIFWKNLSP

tigation was undertaken on Protobind alkali lignin treated with SpMnSOD1 and H_2O_2 in aqueous buffer.

In order to assess the proportion of lignin units involved only in β-aryl ether bonds, thioacidolysis was applied to the lignin samples before and after SpMnSOD1 treatment. The S/G ratio was found to be 1.14 in both cases, indicating that no major structural modification of the lignin polymeric backbone had taken place, which was consistent with the apparent absence of depolymerization observed by GPC. This result suggested that the changes in solubility might be caused by oxidative demethylation of methoxy groups in lignin units to hydroxyl groups. The hydroxyl content of lignin can be assessed experimentally by phosphitylation of free hydroxyl groups (see Figure 4A), followed by ^{31}P NMR spectroscopy, in which the integration and chemical shift of the resulting NMR signals estimate the content of hydroxyl groups and its classification into aliphatic OH, phenolic OH (S type, G type, H type), and carboxyl OH.[22] After treatment with SpMnSOD1

DOI: 10.1021/acschembio.8b00557
ACS Chem. Biol. 2018, 13, 2920−2929

and H_2O_2, analysis by ^{31}P NMR spectroscopy revealed 20−40% increases in aliphatic OH and phenolic OH (see Figure 4B) and a slight increase in carboxyl OH content, consistent with oxidative demethylation (phenolic G, S OH). The increase in total OH content was supported by FT-IR analysis of treated versus untreated lignin samples, which also showed increases of the 3300−3400 cm^{-1} band (see Supporting Information Figure S24).

In contrast, recombinant *Pseudomonas putida* manganese superoxide dismutase SodA, which did not exhibit lignin modification, showed either no change or 5−10% decreases in OH content. Thus, the increased solubility of the lignin after SpMnSOD1 treatment was assigned to increased OH content due to oxidative demethylation.

Identification of Amino Acid Residues in SpMnSOD1 Responsible for Demethylation Activity. Although the crystal structure of SpMnSOD1 revealed that the active site in the vicinity of the Mn(II) cofactor was essentially superimposable upon that of *E. coli* MnSOD,[10] an amino acid sequence alignment of SpMnSOD1 (see Table 2) showed the presence of some amino acid replacements close to Mn(II) binding ligands, which are located in the vicinity of the active site (see Figure 5). Adjacent to Mn(II) ligand His-26, a conserved His-27 residue is replaced by Tyr, and conserved His-31 that is situated close in space, on the next turn of an α-helical structure, is replaced by Ala in SpMnSOD1. A third replacement close in space to Tyr-27 in SpMnSOD1 is the side chain of a Gln residue found as Leu-4 in EcMnSOD1. A fourth replacement adjacent to Mn(II) ligand His-76 is the replacement of Ser or Ala in bacterial MnSOD sequences by Glu-77 residue in SpMnSOD1. These four residues were therefore selected for site-directed mutagenesis, and SpMnSOD1 mutants Q4L, Y27H, A31H, and E77S were generated, in which each of these four residues was changed to the corresponding residue found in *E. coli* MnSOD1.

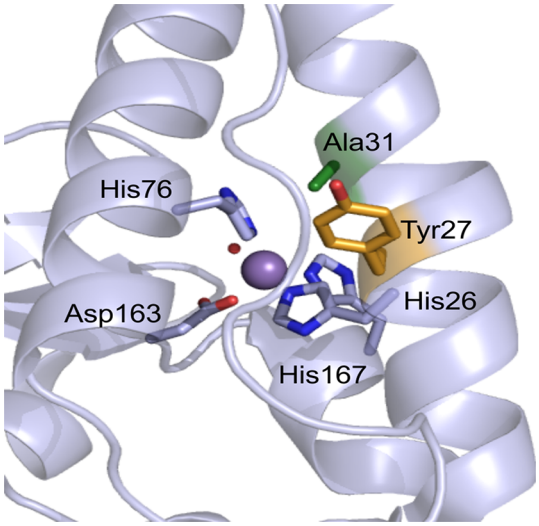

Figure 5. Location of amino acid replacements found in *Sphingobacterium* sp. MnSOD1.

Each of the mutant enzymes was expressed and purified, and the mutant enzymes showed 65−110% of the wild-type superoxide dismutase activity (see Supporting Information Figure S25). Samples of Protobind lignin were treated with each SpMnSOD1 mutant and H_2O_2, and samples were analyzed by ^{31}P NMR spectroscopy as described above. As shown in Figure 4C, treatment by mutants E77S and Q4L gave virtually identical increases in OH content to the wild-type SpMnSOD1 enzyme; however, treatment with mutants A31H or Y27H gave no increases in OH content but, in fact, gave OH content slightly lower than that of untreated lignin. There is therefore a clear difference in behavior between the mutants, indicating that both Ala-31 and Tyr-27 are essential for demethylation activity. The 20−30% decrease in OH content in these mutants might be due to some repolymerization of the lignin, and we note that 5−10% decrease in OH content was observed for *P. putida* SodA, compared with untreated samples. Assay of mutants A31H and Y27H with the hydroxyphenyl-fluorescein in the presence of hydrogen peroxide showed no significant reaction above background (see Figure 3), indicating that these mutants do not generate hydroxyl radical, and no production of protocatechuic acid from vanillic acid was detected for either mutant enzyme *via* HPLC analysis.

The Y27H (PDB code: 6GSB) and A31H (PDB code: 6GSC) SpMnSOD mutant enzymes were then crystallized, and their structures were determined by X-ray crystallography to a resolution of 1.37 and 1.32 Å, respectively. Mutants show a very high level of structural identity with the wild-type with a global rmsd of 0.20 (over 206 CA atoms) and 0.20 (over 205 CA atoms) for Y27H and A31H, respectively (Figure 6).

Superposition of the structures of A31H and Y27H SpMnSOD1 mutants on the structure of wild-type SpMnSOD1 highlighted a shift between the N-terminal loop and the parallel α-helix.[23] There are two points where the distance between the N-terminal loop and parallel α-helix are most notably altered in the mutants compared to wild-type (Figure 7). The first shift is only observed in the Y27H mutant where there is a widening between residue H/Y27 on the α-helix and residues P6/L7 on the N-terminal loop (Figure 6B) amounting to a 0.7 Å increase in the distance compared to the wild-type (Table 3). At the second position, there is a narrowing between residue A/H31 on the α-helix and residue Q4 on the N-terminal loop. This narrowing is more substantial (∼2 Å decrease compared to wild-type) than the difference observed at the first position and interestingly occurs in both the Y27H and A31H mutant.

This alteration in the interaction between the N-terminal loop and the parallel α-helix does not significantly alter the positioning of the Mn coordination or "gateway" residues.[24,25] Solvent channels in the wild-type and mutants were modeled using BetaCavityWeb.[26] This analysis showed a major solvent channel between the two monomers in the wild-type and mutants. The solvent channel situated in the middle of the homodimer has previously been shown to be important in the structure and function of SOD enzymes.[24,25] A modest narrowing for the bottleneck of this solvent channel was observed for the mutants compared to the wild-type (Table 4). Further analysis of channels originating from the pocket between the dimers were calculated using CAVER (Supporting Information Figure S26).[27] This analysis showed the number of calculated channels decreased in the mutants compared to wild-type, with eight predicted channels in the wild-type compared to seven for both the A31H and Y27H mutant. These observations might suggest a decrease in solvent accessibility for the mutants compared to the wild-type. We hypothesize that the observed change in the interaction between the N-terminal loop and the parallel α-helix within these mutants causes a slight alteration in the orientation of

DOI: 10.1021/acschembio.8b00557
ACS Chem. Biol. 2018, 13, 2920−2929

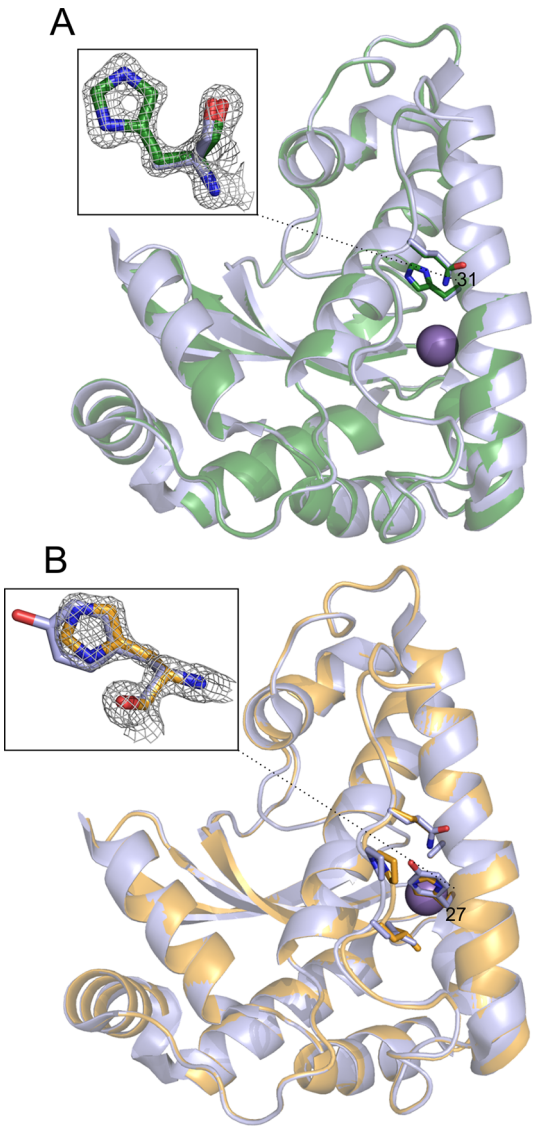

Figure 6. Superposition of SpMnSOD1 wild-type with mutants A31H (A) and Y27H (B). Manganese ions are depicted as purple spheres. Residues with altered conformation between wild-type and mutant are depicted as stick models. Density (σ level 2) shown for residue 31 for A31H and for residue 27 for Y27H, with comparable residues in the wild-type depicted alongside.

this α-helix, resulting in a small shift in several residues, including those involved in the solvent channel.

DISCUSSION

The involement of *Sphingobacterium* sp. T2 manganese superoxide dismutase enzymes in lignin oxidation[10] is unusual because manganese superoxide dismutase is normally involved in protection against oxidative stress, hence it was of particular interest to elucidate the catalytic mechanism for this reaction. In this paper, we provide evidence that treatment of polymeric lignin with SpMnSOD1 causes increases in phenolic OH content, consistent with oxidative demethylation, a reaction observed with vanillic acid (**3**) and observed previously with guaiacol.[10] We have elsewhere observed by FT-IR spectroscopy increases in O−H stretch of polymeric lignin treated with the host bacterium *Sphingobacterium* sp. T2[28] that are consistent with demethylation activity. Increases in aliphatic

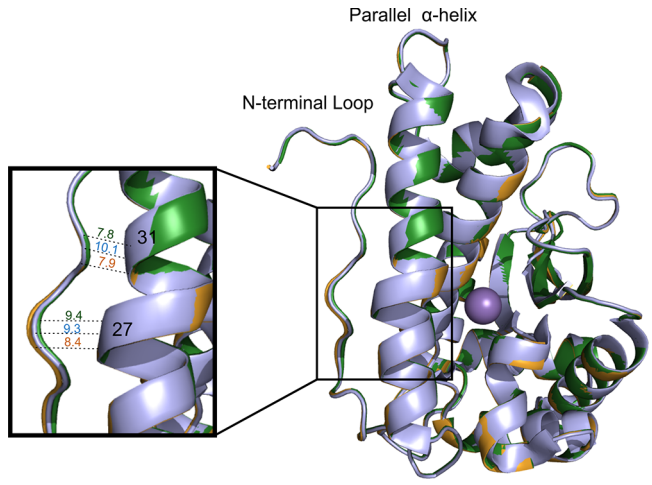

Figure 7. Superposition of SpMnSOD1 wild-type (light blue), A31H (green) and Y27H (orange) mutants. Distance between N-terminal loop and parallel α-helix are shown in blown up image.

Table 3. Distances in Angstroms between the N-Terminal Loop and Parallel α-Helix Measured between the Carbon Backbones at the Two Mutation Points

	distance of Y/H27 to P6 (Å)	distance of A/H31 to Q4 (Å)
SpMnSOD1 wild-type	9.3	10.1
Y27H SpMnSOD1	10.3	8.2
A31H SpMnSOD1	9.4	7.8
E. coli SOD	8.7	7.3

Table 4. Calculated Bottlenecks for the Major Solvent Channel in SpMnSOD1 Wild-Type and Mutants by Betacavityweb[19]

	channel bottleneck (Å)
SpMnSOD1 wild-type	1.432
Y27H SpMnSOD1	1.413
A31H SpMnSOD1	1.409

OH content were also observed by ^{31}P NMR spectroscopy, which would not be explained by oxidative demethylation, suggesting that some interunit bond cleavage reactions are also taking place. The observed reaction of pinoresinol **8** with SpMnSOD1 releases alcohol **10**, hence oxidative cleavage of $\beta-\beta$ linkages found in polymeric lignin might explain the observed increases in aliphatic OH content. These structural changes do not affect the average molar mass of the lignin but would have the effect of solubilizing the polymeric lignin, as we previously observed.[10] Solubilization of lignin content in lignocellulose *in vivo* would allow attack by soil bacteria on the cellulose and hemicellulose polysaccharides of lignocellulose and could be an valuable biotechnological method for lignin solubilization.

SpMnSOD1 is also shown to catalyze a range of oxidative reaction types on lignin model compounds, including aryl−Cα and Cα−Cβ oxidative cleavage, aromatic ring cleavage, phenolic hydroxylation, alcohol side chain oxidation, and dihydroxylation of an alkene side chain, consistent with the generation of a highly reactive oxidant. Moreover, the aryl−Cα and Cα−Cβ oxidative cleavage reactions of lignin model compound **1** were shown to involve ^{18}O incorporation from

DOI: 10.1021/acschembio.8b00557
ACS Chem. Biol. 2018, 13, 2920−2929

$H_2{}^{18}O_2$, and we have provided evidence for the release of 4.1 molar equiv of hydroxyl radical by SpMnSOD1, providing a molecular mechanism for this reactivity. Hydroxyl radical is known to cause phenol hydroxylation,[29] demethylation reactions,[30] and addition reactions of alkenes,[31] so the observed reactions are each consistent with the generation of hydroxyl radical as a reactive oxidant by SpMnSOD1. We therefore propose that hydroxyl radical is generated in SpMnSOD1 by one-electron reduction of hydrogen peroxide, as shown in Figure 8, which then acts as a diffusible oxidant to

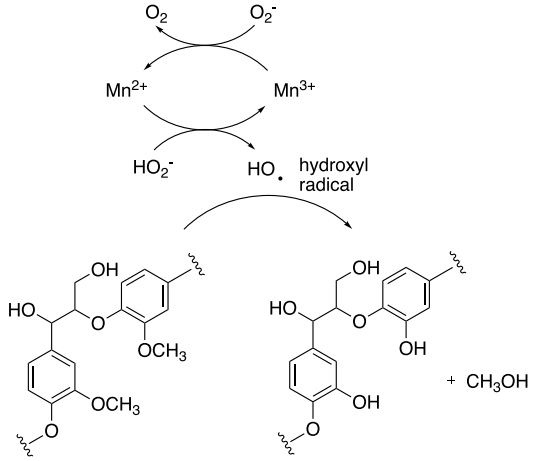

Figure 8. Generation of hydroxyl radical by SpMnSOD1 and demethylation of lignin units.

demethylate lignin, and we have shown that the byproduct of this reaction is methanol, formed *via* an *ipso* substitution by hydroxyl radical. Generation of hydroxyl radical from hydrogen peroxide has also been reported previously in copper−zinc superoxide dismutase, although not in *E. coli* manganese superoxide dismutase.[13] Possible mechanisms involving hydroxyl radical for oxidation of DDVA and pinoresinol by SpMnSOD1 are shown in Supporting Information (Figures S28 and S29).

The molecular basis for this remarkable change in function of this enzyme is shown to involve two point mutations in SpMnSOD1: replacement of His-31 found in *E. coli* MnSOD to Ala and replacement of His-27 to Tyr. The structures of A31H and Y27H mutants of SpMnSOD1 show changes in structure in an N-terminal protein loop near the active site, causing a change in the angle of helix 1 at the dimer interface. There are known to be extensive interactions at the dimer interface of manganese superoxide dismutase that are important for catalysis,[24,25] including Tyr-34 close to the residues implicated here, which is the proton donor for catalytic turnover.[32] Widening of the solvent channel at the dimer interface would facilitate solvent access to the Mn(II) center (see Supporting Information Figure S24), which would be needed in order to deliver protons for hydroxyl radical formation. It is likely that these two mutations would also change the charge balance at the active site, which would alter the redox potential of the Mn(II) center. Alignment of SpMnSOD sequences from a range of bacteria (see Supporting Information Figure S30) indicates that these two mutations are not found in MnSOD sequences from bacterial lignin-degrading strains such as *Rhodococcus jostii* RHA1 and *Pseudomonas putida* KT2440, indicating that those organisms probably do not use this strategy for lignin oxidation. The H27Y mutation is observed in some other Gram-negative bacteria such as *Pseudomonas fluorescens*, *Comamonas testosteroni*, and *Burkholderia xenovorans*, but replacement of both residues is only observed within the Bacteroides phylum, with *B. thetaiotaomicron* containing H27Y and H31L mutations.

Sphingobacterium sp. T2 also produces a second extracellular manganese superoxide enzyme, which also has lignin oxidation activity.[10] The sequence of this enzyme does not contain either of the point mutations noted above; however, it does contain a deletion of 46 amino acids at the N-terminus, relative to SpMnSOD1, and 23 amino acids relative to *E. coli* MnSOD (see Table 2). The Pro-6 and Leu-7 residues that are altered in position in SpMnSOD1 are therefore completely absent in SpMnSOD2, hence this N-terminal deletion would completely remove the N-terminal loop, and we hypothesize that this would increase solvent access to the Mn center *via* a different structural change. Therefore, it appears that there are two different solutions to this change in activity that are present in the same organism. The biological production of hydroxyl radical in SpMnSOD1 is a remarkable mechanism but illustrates the powerful oxidative chemistry needed to attack the chemically inert lignin structure, such as the Fenton chemistry used in brown-rot fungi and the intriguing solutions that Nature has found to achieve this feat.

EXPERIMENTAL SECTION

Enzyme Purification. Gene-encoding *SpMnSOD1* enzyme has been cloned without signal peptide using forward 5′-CACCCA-ATTTAAACAGACCC-3′ and reverse 5′-TTATTTTTTCAA-GGCTTTCTCATATCG-3′ primers and transformed into *E. coli* BL21 strain. The enzyme was overexpressed (using 1 mM IPTG) from recombinant plasmid (pET151 containing mature SpMn*SOD1*). The His-tagged protein purified to near homogeneity by using immobilized ion affinity chromatography (IMAC) under native conditions (Ni-NTA column, Qiagen), as described previously.[10]

Site-Directed Mutagenesis of SpMnSOD1. Site-directed mutagenesis was carried out using the QuikChange II XL site-directed mutagenesis kit (Agilent), following the manufucturer's instructions, using PfuUltra HF DNA polymerase. Primers used for SpSOD1 site-directed mutagenesis were as follows:

Q4L forward: 5′-gacgacatttgcacaatttaaactgaccccacttccatatg-3′
Reverse: 5′-catatggaagtggggtcagtttaaattgtgcaaatgtcgtc-3′
Y27H forward: 5′-gaccatggagatccaccacagcaagcatgctgc-3′
Reverse: 5′-gcagcatgcttgctgtggtggatctccatggtc-3′
A31H forward: 5′-atggagatccactacagcaagcatcatgcaggatatacgg-3′
Reverse: 5′-ccgtatatcctgcatgatgcttgctgtagtggatctccat-3′
E77S forward: 5′-cgggaggccactacaaccacagcctgttttggtctatcctaac-3′
Reverse: 5′-gttaggatagaccaaaacaggctgtggttgtagtggcctcccg-3′

Transformation of Lignin Model Compounds. Lignin dimer model compounds (1.6 mM final concentration) and monocyclic aromatic compounds (16 mM final concentration) were incubated with SpMnSOD1 (final concentration 8−10 μM) in 2.5 mL of 50 mM NH_4HCO_3 buffer pH 7.8 containing 1.6 mM EDTA, to which 1 mL of saturated KO_2/DMSO under N_2 was added. After 1 h, 1 mL of 1 M HCl was added to stop the reaction.

Samples for LC/MS analysis (0.5 mL) were extracted with ethyl acetate (1 mL) and then evaporated under reduced pressure. The organic residues were redissolved in 1:1 MeOH/H_2O and injected onto a reverse-phase Phenomenex Luna 5 μm C_{18} column (100 Å, 50 mm, 4.6 mm) on an Agilent 1200 and Bruker HCT Ultra mass spectrometer, at a flow rate of 0.5 mL/min, and monitored at 310 and 270 nm. The solvent system was water (A) and MeOH (B) containing 1% formic acid (for positive ionization mode), starting with 5% of buffer B, then the following gradient: 0−30% B over 0−20 min; 30% B for 10 min; 30−100% B from 30 to 45 min; 100% B for 8 min; 100−5% B for 8 min.

DOI: 10.1021/acschembio.8b00557
ACS Chem. Biol. 2018, 13, 2920−2929

Samples for GC/MS analysis (0.5 mL) were extracted with ethyl acetate (1 mL) and then evaporated under reduced pressure. The residues were reconstituted with dry chloroform (1 mL), dried ($MgSO_4$), and then either analyzed directly by GC-MS or silylated with *N*,*O*-bis(trimethylsilyl)acetamide. Silylation reaction for GC-MS was carried out by mixing 200 μL of samples in dry solvent with 100 μL of silylation mixture of chlorotrimethylsilane, *N*,*O*-bis-(trimethylsilyl)acetamide (1:20), and 200 μL of pyridine at 60 °C for 1 h and diluted 10-fold. The analysis was performed using a gas chromatograph−mass spectrometer (GC/MS/MS, Varian 4000) on a Varian Factor Four column (length = 30 m, i.d. = 0.25 mm, thickness = 0.25 μm). Electron impact mass spectra (EI-MS) were recorded at ionization energy of 70 eV. The temperature gradient was as follows: 50 °C for 1 min; 50−300 °C at the rate of 7.5 °C per minute; maintained at 300 °C for 5.67 min.

^{18}O Labeling Experiment. In a 20 mL glass vessel containing 4 mL of phosphate buffer (50 mM, pH 7), lignin model compound guaiacylglycerol-β-guaiacyl ether (1 mM final concentration) was incubated with SpMnSOD1 (10−20 μM) and glucose oxidase from *Aspergillus niger* (50−100 U/mL). The vessel was degassed with nitrogen and then saturated with $^{18}O_2$ gas (Cambridge Isotope Laboratories), and glucose solution (1 mM final concentration, degassed under N_2) was added. After 1 h, the products were extracted with EtOAc and analyzed by GC-MS.

GPC Analysis. Organosolv lignin (1.66 mg) was added to 1 mL of 50 mM phosphate buffer (pH 7.8, with 0.1 mM EDTA), then 2.6 μL of 1 M hydrogen peroxide was added, followed by 0.4 mg of purified SpMnSOD1. The reaction incubated at 30 °C for 4 h. After the reaction, 250 μL of 1 M HCl was added to each sample to terminate the enzymatic reaction. Samples were centrifuged (12 000 rpm, microcentrifuge) for 10 min and then subjected to GPC analysis in DMF. A control incubation contained enzyme premixed with 250 μL of 1 M HCl.

Quantitative ^{31}P NMR and Sample Preparation. To prepare samples for ^{31}P NMR experiment, 100 mg of Protobind alkali lignin (Green Value Ltd.) was dissolved in 40 mL of 50 mM phosphate buffer pH 7.8 containing 0.1 mM EDTA. Then 2.0 mg of purified SpMnSOD1 was added, and 2.6 μL of 1 M hydrogen peroxide was added to initiate the reaction. The reactions were incubated at 30 °C for 2 h. Next, 1.6 mL of 1 M HCl was added to terminate the reaction and precipitate the enzyme and lignin. The samples were then freeze-dried. A control reaction containing no enzyme was also carried out, abnd reactions were carried out in duplicate.

Derivatization of the lignin samples with 2-chloro-4,4′,5,5′-tetramethyl-1,3,2-dioxaphospholane (TMDP, Sigma-Aldrich, France) was performed according to Granata *et al.*[22] Lignin samples (approximately 20 mg) were dissolved in 400 μL of a mixture of anhydrous pyridine and deuterated chloroform (1.6:1 v/v). Then 150 μL of a solution containing cyclohexanol (4.05 mg mL^{-1}) and chromium(III) acetylacetonate (3.90 mg mL^{-1}) was added, which served as an internal standard and relaxation reagent, respectively, and 75 μL of TMDP. NMR spectra were acquired on a Bruker Biospin Avance III 400 MHz spectrometer. A total of 128 scans were acquired with a delay time of 6 s between successive pulses. The spectra were processed using Topspin 3.1. All chemical shifts are reported relative to the product of TMDP with cyclohexanol, which has been observed to give a doublet at 145 ppm referenced from the water−TMDP signal (132.2 ppm). The content of the hydroxyl groups (in mmol g^{-1}) was calculated on the basis of hydroxyl groups contained in the internal reference cyclohexanol and by integration of the following spectral regions: aliphatic hydroxyls (151−146 ppm), syringyl phenolic hydroxyls (144−141 ppm), guaiacyl phenolic hydroxyls (140.5−138.5), *p*-hydroxyphenyl phenolic hydroxyls (138.4−137.0 ppm), and carboxylic acids (136.6−133.6 ppm).

HPF Assay for Hydroxyl Radical Detection. Purified SpMnSOD1 (24−145 μg) was added to a solution of β-aryl ether lignin model compound (100 μM) in 250 μL of 50 mM phosphate buffer pH 8.0 containing 0.1 mM EDTA and 3 μM HPF (Sigma-Aldrich). Then 10 μL of 100 mM hydrogen peroxide was added to generate a signal. Two hundred microliter of the reaction mixture was monitored in a Hidex 96-well microtiter plate reader (excitation wavelength = 485 nm; emission wavelength = 535 nm) and monitored at 30 s intervals for 10 min. Calibration was carried out using 5−40 μM ammonium iron(II) sulfate with 3 μM HPF in 250 μL of 50 mM phosphate buffer pH 7.5. Then 2.5 μL of 100 mM hydrogen peroxide was added to generate hydroxyl radical, and the reaction was monitored as above.

Detection of Co-products of the SpMnSOD Reaction. Formaldehyde as a possible product was analyzed from vanillic acid and 1,4-dimethoxybenzene (1 mM final concentration) as substrates with purified SpMnSOD1 (100 μg) in 50 mM phosphate buffer pH 8.0 at 30 °C, with acetoacetanilide in the presence of ammonia using the method of Li *et al.*[20] Samples (20 μL) were added to microtiter plates containing ethanolic acetoacetanilide (80 μL of 100 mM solution), to which 100 μL of ammonium acetate (4 M) was added. The signals were monitored monitored using Hidex microtiter plate reader (excitation wavelength = 355/40 nm; emission wavelength = 460/20 nm) at 30 s intervals for 10 min. A series of standard solutions (10, 20, 50, and 100 μM) of formaldehyde (Sigma-Aldrich) were used for calibration.

Methanol as a possible product was analyzed by the method of Barrett,[21] *via* conversion to formaldehyde using alcohol oxidase from *Pichia pastoris*, Sigma-Aldrich), and formaldehyde was determined as described above. Samples (20 μL) initially incubated with alcohol oxidase (5 μL of 100 U) in 100 μL of 50 mM phosphate buffer pH 7.5 at 30 °C, and then 20 μL was taken for formaldehyde determination as above. A series of standard solutions of methanol (20, 40, 60, 80, and 100 μM) were used for calibration.

The amount of remaining hydrogen peroxide from the reaction of SpMnSOD1 with vanillic acid was determined using 2,4-dichlorophenol (2,4-DCP) and peroxidase enzyme (Dyp 1B from *Pseudomonas fluorescens*).[6] Samples (20 μL) were added to microtiter plate wells containing 5 μL of 2,4-DCP (100 mM), 5 μL of 4-aminoantipyrine (35 mM), and 2 μL of Dyp 1B in 200 μL of potassium acetate (50 mM) buffer pH 5.5. The absorbance was monitored using Hidex microtiter plate reader at 510 nm for 10 min. A series of solutions of hydrogen peroxide (5, 10, 15, 30, 60, and 120 μM) were used for calibration.

Structure Determination of Y27H and A31H Mutant Enzymes. Pure recombinant Y27H SpMnSOD1 mutant (20 mg mL^{-1}) and A31H SpMnSOD1 mutant (17 mg mL^{-1}) in 20 mM Tris pH 8 were subjected to manual crystallization screening using 24-well screens designed around crystallization conditions found for the wild-type.[10] One microliter of protein was mixed with 1 μL of crystallization solution. Plates were incubated at 18 °C, and small rod-shaped crystals appeared after 3−4 months. Y27H crystals grew in 160 mM ammonium citrate dibasic, 26% PEG 3350, and A31H crystals grew in 130 mM ammonium citrate, 26% PEG 3350. Crystals were removed from drops using a mounted Litholoop (Molecular Dimensions), cryoprotected in crystallization solution containing 10% ethylene glycol/glycerol for Y27H and 15% ethylene glycol for A31H, and flash-frozen in liquid nitrogen.

X-ray diffraction data to a resolution of 1.37 Å for Y27H and 1.32 Å for A31H were collected at 100 K at the beamline I03 at the Diamond Light Source, U.K. using a Pilatus 6 M detector. All data were indexed, integrated, and scaled using the XDS package.[33] Further data handling was carried out using the CCP4 software package.[34] Refinement of the structure was carried out by alternate cycles of manual refitting using Coot[35] and Refmac,[36] using the initial model of the isomorphous wild-type structure (PDB code: 5a9g).[10] Water molecules were added to the atomic model automatically using ARP,[37] at the positions of large positive peaks in the difference electron density, only at places where the resulting water molecule fell into an appropriate hydrogen bonding environment. Restrained isotropic temperature factor refinements were carried out for each individual atom. The polypeptide chain was traced through electron density maps ($2F_o - F_c$ and $F_o - F_c$), for residues −4 to 201 for mutant Y27H and residues −2 to 202 for mutant A31H. Data collection and refinement statistics are given in Table 5.

DOI: 10.1021/acschembio.8b00557
ACS Chem. Biol. 2018, 13, 2920−2929

Table 5. Crystallography Data Collection and Refinement Statistics

	Y27H	*A31H*
Data Collection[a]		
space group	$P2_1$	$P2_1$
cell dimensions		
a, *b*, *c* (Å)	46.68, 59.09, 75.21	46.53, 58.61, 75.07
α, *β*, *γ* (deg)	90, 90.47, 90	90, 90.37, 90
wavelength (Å)	0.97948	0.97623
resolution (Å)	37−1.45 (1.53−1.45)	40−1.32 (1.39−1.32)
observations	368354 (52448)	937258 (132118)
unique reflections	71340 (5108)	94757 (6973)
R_{sym}	0.065 (0.569)	0.090 (0.951)
$I/\sigma(I)$	13.7 (2.1)	14.3 (2.0)
completeness (%)	98.5 (97.1)	100.0 (100.0)
redundancy	5.2 (5.1)	9.9 (9.6)
Refinement		
R_{cryst}	0.149 (0.283)	0.150 (0.243)
reflections used	68524 (4922)	90988 (6698)
R_{free}	0.169 (0.290)	0.166 (0.256)
reflections used	2816 (186)	3769 (275)
R_{cryst} (all data)	0.150	0.151
non-hydrogen atoms	3872 (including 2 Mn^{2+} and 628 waters)	3839 (including 2 Mn^{2+} and 529 waters)
B-factors		
protein	8.3	16.5
water	33.5	32.2
rms deviations		
bond lengths (Å)	0.014	0.014
bond angles (deg)	1.6	1.6
DPI coordinate error (Å)	0.060	0.045

[a]Values in parentheses are for highest-resolution shell.

■ ASSOCIATED CONTENT

Supporting Information

The Supporting Information is available free of charge on the ACS Publications website at DOI: 10.1021/acschembio.8b00557.

GC-MS and LC-MS spectra of SpMnSOD1 reaction products, supporting biochemical assay data, GPC and FT-IR data, and supporting crystallographic data (PDF)

■ AUTHOR INFORMATION

Corresponding Author

*E-mail T.D.Bugg@warwick.ac.uk. Tel: 44-2476 573018.

ORCID

Timothy D. H. Bugg: 0000-0003-3964-4498

Author Contributions

⊥G.M.M.R. and X.Z. contributed equally to the work described in the paper.

Notes

The authors declare no competing financial interest.

■ ACKNOWLEDGMENTS

This work was supported by BBSRC research Grants BB/M025772/1 and BB/M003523/1. This project has received funding from the Bio-Based Industries Joint Undertaking under the European Union Horizon 2020 research and innovation programme under Grant Agreement 720303 and was supported in part by a Ph.D. studentship (to G.M.M.R.) funded by the Kurdistan Regional Government (KRG) Ministry of Higher Educarion and Scientific Research. The IJPB benefits from the support of the LabEx Saclay Plant Sciences-SPS (ANR-10-LABX-0040-SPS). Crystallographic data were collected at beamline I03 at Diamond Light Source, U.K., and we acknowledge the support of beamline scientists K. McAuley and M. Williams.

■ REFERENCES

(1) Zakzeski, J., Bruijnincx, P. C., Jongerius, A. L., and Weckhuysen, B. M. (2010) The catalytic valorization of lignin for the production of renewable chemicals. *Chem. Rev. 110*, 3552−3599.

(2) Wong, D. W. S. (2009) Structure and action mechanism of lignolytic enzymes. *Appl. Biochem. Biotechnol. 157*, 174−209.

(3) Bugg, T. D. H., Ahmad, M., Hardiman, E. M., and Singh, R. (2011) The emerging role for bacteria in lignin degradation and bio-product formation. *Curr. Opin. Biotechnol. 22*, 394−400.

(4) Ahmad, M., Roberts, J. N., Hardiman, E. M., Singh, R., Eltis, L. D., and Bugg, T. D. H. (2011) Identification of DypB from *Rhodococcus jostii* RHA1 as a lignin peroxidase. *Biochemistry 50*, 5096−5107.

(5) Brown, M. E., Barros, T., and Chang, M. C. Y. (2012) Identification and characterization of a multifunctional dye peroxidase from a lignin-reactive bacterium. *ACS Chem. Biol. 7*, 2074−2081.

(6) Rahmanpour, R., and Bugg, T. D. H. (2015) Characterisation of Dyp-type peroxidases from *Pseudomonas fluorescens* Pf-5: oxidation of Mn(II) and polymeric lignin by Dyp1B. *Arch. Biochem. Biophys. 574*, 93−98.

(7) Majumdar, S., Lukk, T., Solbiati, J. O., Bauer, S., Nair, S. K., Cronan, J. E., and Gerlt, J. A. (2014) Roles of small laccases from *Streptomyces* in lignin degradation. *Biochemistry 53*, 4047−4058.

(8) Granja-Travez, R. S., Wilkinson, R. C., Persinoti, G. F., Squina, F. M., Fülöp, V., and Bugg, T. D. H. (2018) Structural and functional characerisation of multi-copper oxidase CueO from lignin-degrading bacterium *Ochrobactrum* sp. reveal its activity towards lignin model compounds and lignosulfonate. *FEBS J. 285*, 1684−1700.

(9) Taylor, C. R., Hardiman, E. M., Ahmad, M., Sainsbury, P. D., Norris, P. R., and Bugg, T. D. H. (2012) Isolation of bacterial strains able to metabolise lignin from screening of environmental samples. *J. Appl. Microbiol. 113*, 521−530.

(10) Rashid, G. M. M., Taylor, C. R., Liu, Y., Zhang, X., Rea, D., Fülöp, V., and Bugg, T. D. H. (2015) Identification of manganese superoxide dismutase from *Sphingobacterium* sp. T2 as a novel bacterial enzyme for lignin oxidation. *ACS Chem. Biol. 10*, 2286−2294.

(11) Pick, M., Rabani, J., Yost, F., and Fridovich, I. (1974) Catalytic mechanism of the manganese-containing superoxide dismutase of *Escherichia coli* studied by pulse radiolysis. *J. Am. Chem. Soc. 96*, 7329−7333.

(12) Ludwig, M. L., Metzger, A. L., Pattridge, K. A., and Stallings, W. C. (1991) Manganese superoxide dismutase from *Thermus thermophilus*:a structural model refined at 1.8 Å resolution. *J. Mol. Biol. 219*, 335−358.

(13) Yim, M. B., Chock, P. B., and Stadtman, E. R. (1990) Copper, zinc superoxide dismutase catalyzes hydroxy radical production from hydrogen peroxide. *Proc. Natl. Acad. Sci. U. S. A. 87*, 5006−5010.

(14) Hyde, S. M., and Wood, P. M. (1997) A mechanism for production of hydroxyl radicals by the brown-rot fungis *Coniophora puteana*: Fe(III) reduction by cellulose dehydrogenase and Fe(II) oxidation at a distance from the hyphae. *Microbiology 143*, 259−266.

(15) Kerem, Z., Jensen, K. A., and Hammel, K. E. (1999) Biodegradative mechanism of the brown rot basidiomycete *Gloeophyllum trabeum*: evidence for an extracellular hydroquinone-driven Fenton reaction. *FEBS Lett. 446*, 49−54.

DOI: 10.1021/acschembio.8b00557
ACS Chem. Biol. 2018, 13, 2920−2929

(16) Price, M., Reiners, J. J., Santiago, A. M., and Kessel, D. (2009) Monitoring singlet oxygen and hydroxyl radical formation with fluorescent probes during photodynamic therapy. *Photochem. Photobiol. 85*, 1177−1181.
(17) Adams, G. E., Boag, J. W., and Michael, B. D. (1965) Reactions of the hydroxyl radical. *Trans. Faraday Soc. 61*, 1674−1680.
(18) Hardwick, T. J. (1957) The rate constant of the reaction between ferrous ions and hydrogen peroxide in acid solution. *Can. J. Chem. 35*, 428−436.
(19) O'Neill, P., Schulte-Frohlinde, D., and Steenken, S. (1977) Formation of radical cations and zwitterions versus demethoxylation in the reaction of hydroxyl radical with a series of methoxylated benzenes and benzoic acids. *Faraday Discuss. Chem. Soc. 63*, 141−148.
(20) Li, Q., Sritharathikhun, P., and Motomizu, S. (2007) Development of novel reagent for Hantzsch reaction for the determination of formaldehyde by spectrophotometry and fluorometry. *Anal. Sci. 23*, 413−417.
(21) Anthon, G. E., and Barrett, D. M. (2004) Comparison of three colorimetric reagents in the determination of methanol with alcohol oxidase: application to the assay of pectin methylesterase. *J. Agric. Food Chem. 52*, 3749−3753.
(22) Granata, A., and Argyropoulos, D. S. (1995) 2-Chloro-4,4,5,5-tetramethyl-1,3,2-dioxaphospholane, a reagent for the accurate determination of the uncondensed and condensed phenolic moieties in lignin. *J. Agric. Food Chem. 43*, 1538−1544.
(23) Maiti, R., Van Domselaar, G. H., Zhang, H., and Wishart, D. S. (2004) SuperPose: a simple server for sophisticated structural superposition. *Nucleic Acids Res. 32*, W590−594.
(24) Edwards, R. A., Whittaker, M. M., Whittaker, J. W., Baker, E. N., and Jameson, G. B. (2001) Outer sphere mutations perturb metal reactivity in manganese superoxide dismutase. *Biochemistry 40*, 15−27.
(25) Whittaker, M. M., and Whittaker, J. W. (1998) A glutamate bridge is essential for dimer stability and metal stability and metal selectively in manganese superoxide dismutase. *J. Biol. Chem. 273*, 22188−22193.
(26) Kim, J.-K., Cho, Y., Lee, M., Laskowski, R. A., Ryu, S. E., Sugihara, K., and Kim, D. S. (2015) BetaCavityWeb: a webserver for molecular voids and channels. *Nucleic Acids Res. 43*, W413−418.
(27) Chovancova, E., Pavelka, A., Benes, P., Strnad, O., Brezovsky, J., Kozlikova, B., Gora, A., Sustr, V., Klvana, M., Medek, P., Biedermannova, L., Sochor, J., and Damborsky, J. (2012) CAVER 3.0: A Tool for Analysis of Transport Pathways in Dynamic Protein Structures. *PLoS Comput. Biol. 8*, 10.
(28) Konstantopoulou, M., Slator, P. J., Taylor, C. R., Wellington, E. M., Allison, G., Harper, A. L., Bancroft, I., and Bugg, T. D. H. (2017) Variation in susceptibility to microbial lignin oxidation in a set of wheat straw cultivars: influence of genetic, seasonal and environmental factors. *Nord. Pulp Pap. Res. J. 32*, 493−507.
(29) Grootveld, M., and Halliwell, B. (1986) Aromatic hydroxylation as a potential measure of hydroxyl radical formation *in vivo*: identification of hydroxylated derivatives of salicylate in human body fluids. *Biochem. J. 237*, 499−504.
(30) Fraser-Reid, B., Jones, J. K. N., and Perry, M. B. (1961) The demethylation of sugars with hydrogen peroxide. *Can. J. Chem. 39*, 555−563.
(31) Griffiths, W. E., Longster, G. F., Myatt, J., and Todd, P. F. (1967) The electron spin resonance spectra of radicals obtained by addition of amino and hydroxyl radicals to alkenes. *J. Chem. Soc. B*, 530−533.
(32) Whittaker, M. M., and Whittaker, J. W. (1997) Mutagenesis of a proton linkage pathway in *Escherichia coli* manganese superoxide dismutase. *Biochemistry 36*, 8923−8931.
(33) Kabsch, W. (2010) XDS. *Acta Crystallogr., Sect. D: Biol. Crystallogr. 66*, 125−132.
(34) Dodson, E. J., Winn, M., and Ralph, A. (1997) Collaborative computational project, number 4: Providing programs for protein crystallography. *Methods Enzymol. 277*, 620−633.
(35) Emsley, P., and Cowtan, K. (2004) Coot: model-building tools for molecular graphics. *Acta Crystallogr., Sect. D: Biol. Crystallogr. 60*, 2126−2132.
(36) Murshudov, G. N., Vagin, A. A., and Dodson, E. J. (1997) Refinement of macromolecular structures by the maximum-likelihood method. *Acta Crystallogr., Sect. D: Biol. Crystallogr. 53*, 240−255.
(37) Langer, G. G., Cohen, S. X., Lamzin, V. S., and Perrakis, A. (2008) Automated macromolecular model building for X-ray crystallography using ARP/wARP version. *Nat. Protoc. 3*, 1171−11795.

DOI: 10.1021/acschembio.8b00557
ACS Chem. Biol. 2018, 13, 2920−2929